





## Effective nonadiabatic holonomic SWAP gate with Rydberg atoms using invariant-based reverse engineering

Yang Xiao <sup>1,2</sup> Yi-Hao Kang <sup>3,1,2</sup> Ri-Hua Zheng,<sup>1,2</sup> Jie Song,<sup>4</sup> Ye-Hong Chen <sup>1,2,5,\*</sup> and Yan Xia <sup>1,2,†</sup>

<sup>1</sup>Fujian Key Laboratory of Quantum Information and Quantum Optics, Fuzhou University, Fuzhou 350108, China

<sup>2</sup>Department of Physics, Fuzhou University, Fuzhou 350108, China

<sup>3</sup>School of Physics, Hangzhou Normal University, Hangzhou 311121, China

<sup>4</sup>Department of Physics, Harbin Institute of Technology, Harbin 150001, China

<sup>5</sup>Theoretical Quantum Physics Laboratory, RIKEN Cluster for Pioneering Research, Wako-shi, Saitama 351-0198, Japan



(Received 4 April 2024; accepted 28 May 2024; published 17 June 2024)

In this paper, we propose a one-step scheme for implementing the nonadiabatic holonomic SWAP gate with Rydberg atoms. By applying invariant-based reverse engineering to design the effective Hamiltonian of the system, a suitable evolution path for implementing nonadiabatic holonomic quantum computation is found. In addition, the systematic-error-sensitivity nullified optimal control method is considered in the parameter selections, so that the scheme is insensitive to the systematic error of pulses. We also estimate the effects of random noise, the random initial phase of the pulses, the Doppler shift, and decoherence on the scheme. The numerical results show that the scheme exhibits fairly good performance against these negative factors. Finally, we generalize the scheme to realize the non-Clifford SWAP gates. Therefore, this scheme can provide a feasible framework for implementing high-fidelity and robust SWAP gates and non-Clifford SWAP gates with Rydberg atoms.

DOI: [10.1103/PhysRevA.109.062610](https://doi.org/10.1103/PhysRevA.109.062610)

### I. INTRODUCTION

Neutral atoms interacting through dipole-dipole interactions have been used to construct promising platforms for quantum computing [1,2]. Rydberg atoms are a kind of neutral atom excited to high-lying Rydberg states, exhibiting significant Rydberg-Rydberg interactions (RRIs) [3]. Neutral Rydberg atoms display the following two distinct dynamics: (1) Once an atom is excited to its Rydberg state, because the linewidth of the excitation is significantly narrower than the energy shift caused by the RRI, other atoms within the blocking radius cannot be excited to the Rydberg state, which is called the Rydberg blockade [4–7]. (2) If the Rabi frequencies are not resonant, with huge two-photon detunings close to the energy shift of the RRI, an opposite phenomenon occurs: more than one atom is pumped into the Rydberg state, which is known as Rydberg antiblockade [8–13]. These two excitation processes provide promising methods for the construction of quantum logic gates, such as Rydberg blockade gates [14–17] and Rydberg antiblockade gates [18–23].

Although various schemes [24–27] have been proposed to realize a Rydberg-mediated quantum gate, one-step implementations of two-qubit gates or multiqubit gates, especially some commonly used gates (e.g., the SWAP gate and the Fredkin gate [28]), have been discussed in only a few articles. The SWAP gate is an important two-qubit gate which is widely used in quantum computing [29], entanglement swapping [30], and quantum repeaters [31]. The SWAP gate

in existing Rydberg-mediated gate schemes usually involves multiple fragment pulses, requiring three or more steps, and two or more Rydberg states involved in a single Rydberg atom [27,32,33]. The multistep operation of quantum gates makes quantum computing more complicated and increases the sensitivity to errors and noise in quantum computing. Therefore, the one-step implementation of a high-fidelity SWAP gate is more advantageous for the realization of quantum computing in neutral atoms.

For the implementation of high-fidelity quantum gates, the scheme should be robust to experimental interference factors, including systematic errors, random noise, and decoherence. Nonadiabatic holonomic quantum computation (NHQC) has received significant attention in recent years because of its potential to overcome these interference factors [34–38]. First of all, NHQC is not limited by adiabatic conditions, which makes the evolution faster than adiabatic holonomic quantum computation [39–42], thus reducing the influence of decoherence. In addition, NHQC is based on geometric phases, which depend on the global properties of the evolution paths, and, consequently, is insensitive to parameter fluctuations in the process of a cyclic evolution [43–50]. Importantly, recent studies [51–54] have shown that NHQC can significantly enhance the robustness against systematic errors by cooperating with control and optimal methods, such as reverse engineering [55–64] and the systematic-error-sensitivity nullified optimal control method [65–69]. Therefore, realizing high-fidelity and robust quantum gates based on NHQC is promising.

In this paper, we propose a one-step scheme to realize the nonadiabatic holonomic SWAP gate for Rydberg atoms by using invariant-based reverse engineering. The physical system consists of two Rydberg atoms. When the atoms

\*Contact author: [yehong.chen@fzu.edu.cn](mailto:yehong.chen@fzu.edu.cn)

†Contact author: [xia-208@163.com](mailto:xia-208@163.com)

are driven by laser pulses with large detuning, we derive an effective Hamiltonian. Then, invariant-based reverse engineering is applied to design the evolution path of NHQC based on the effective Hamiltonian. We further employ the systematic-error-sensitivity nullified optimal control method [65] to modify the parameters, so that the scheme is robust to systematic errors of the pulses. The validity of the scheme is verified by numerical simulations based on the full Hamiltonian. Meanwhile, we also use numerical simulations to analyze the influence of systematic errors, random noise, the random initial phase of the pulses, the Doppler shift, and decoherence on the scheme. The results show that the scheme maintains relatively high fidelity in the presence of these imperfections. Finally, the scheme is generalized to realize the non-Clifford SWAP gates. Therefore, the scheme may provide an idea for the realization of high-fidelity and robust SWAP gates and their extensions.

This paper is organized as follows. In Sec. II, the protocols for NHQC based on invariant-based reverse engineering are reviewed. In Sec. III, we introduce the model and the Hamiltonian of the system and propose the scheme for the holonomic SWAP gate by combining invariant-based reverse engineering and the systematic-error-sensitivity nullified method. In Sec. IV, the validity of the scheme is proved with numerical simulations, and the influence of systematic errors, random noise, and decoherence on the scheme is analyzed. In Sec. V, we extend the scheme to realize the non-Clifford SWAP gates. Finally, the conclusions are given in Sec. VI.

## II. NON-ADIABATIC HOLONOMIC QUANTUM COMPUTATION WITH INVARIANT-BASED REVERSE ENGINEERING

### A. Lewis-Riesenfeld invariant theory

We first introduce the Lewis-Riesenfeld invariant theory [70]. We consider a system Hamiltonian  $H(t)$  and assume a Hermitian operator  $I(t)$  satisfying the equation ( $\hbar = 1$ )

$$i\frac{\partial}{\partial t}I(t) - [H(t), I(t)] = 0 \quad (1)$$

exists. The Hermitian operator  $I(t)$  is called a dynamic invariant. The solution of the time-dependent Schrödinger equation  $i\dot{|\Psi(t)\rangle} = H(t)|\Psi(t)\rangle$  for the system can be expanded by the nondegenerate eigenvectors  $\{|\psi_l(t)\rangle\}$  of the dynamic invariant  $I(t)$  as

$$|\Psi(t)\rangle = \sum_l c_l |\Phi_l(t)\rangle, \quad |\Phi_l(t)\rangle = \exp[i\alpha_l(t)] |\psi_l(t)\rangle, \quad (2)$$

where  $c_l = \langle \psi_l(0) | \Psi(0) \rangle$  ( $l = 0, 1, 2, \dots$ ) is the correlation coefficient and  $\alpha_l(t)$  is the Lewis-Riesenfeld phase defined as

$$\alpha_l(t) = \int_0^t \langle \psi_l(t') | \left[ i\frac{\partial}{\partial t'} - H(t') \right] | \psi_l(t') \rangle dt'. \quad (3)$$

Therefore, the dynamic invariant  $I(t)$  can be used to analyze the evolution of the system. In addition, by constructing the dynamic invariant  $I(t)$  and making a proper ansatz for its parameters, the Hamiltonian  $H(t)$  also can be derived in reverse via Eq. (1) [71]. Lie algebra is commonly utilized as a foundational approach in the construction of dynamic invariants, providing the necessary algebraic structure and properties that

help in identifying such quantities [72,73]. This methodology not only facilitates a deeper understanding of the systematic dynamics but also enables the determination of the underlying Hamiltonian governing its time evolution.

### B. Nonadiabatic holonomic quantum computation with a dynamic invariant

In this section, we briefly introduce the theory of NHQC with a dynamic invariant. First, we consider a computational subspace  $S$  that can be used to implement NHQC. According to Ref. [51], it is necessary to select a set of time-dependent vectors  $\{|\tilde{\phi}_l(t)\rangle\}$  spanning  $S$  and meet the cyclic evolution condition  $|\tilde{\phi}_l(0)\rangle = |\tilde{\phi}_l(T)\rangle$  ( $T$  is the total operation time). In addition, the operator  $\tilde{\zeta}_l(t) = |\tilde{\phi}_l(t)\rangle\langle\tilde{\phi}_l(t)|$  needs to obey the von Neumann equation

$$\frac{d}{dt}\tilde{\zeta}_l(t) = -i[H(t), \tilde{\zeta}_l(t)]. \quad (4)$$

When the above two conditions are satisfied, the evolution operator in the subspace  $S$  can be described as

$$U(T, 0) = \sum_l e^{i[\tilde{\vartheta}_l(T) + \tilde{\Theta}_l(T)]} \tilde{\zeta}_l(0), \quad (5)$$

with

$$\begin{aligned} \tilde{\vartheta}_l(t) &= -\int_0^t \langle \tilde{\phi}_l(t') | H(t') | \tilde{\phi}_l(t') \rangle dt', \\ \tilde{\Theta}_l(t) &= \int_0^t \langle \tilde{\phi}_l(t') | i\frac{\partial}{\partial t'} | \tilde{\phi}_l(t') \rangle dt', \end{aligned} \quad (6)$$

where  $\tilde{\vartheta}_l(t)$  and  $\tilde{\Theta}_l(t)$  are the dynamic phase and the geometric phase acquired by the vector  $|\tilde{\phi}_l(t)\rangle$  during the time interval  $[0, t]$ , respectively. When  $\tilde{\vartheta}_l(T) = 0$ , a purely geometric phase can be obtained.

Based on the theory in Sec. II A, the nondegenerate eigenvectors of a dynamic invariant can be used as an alternative to the auxiliary vectors  $\{|\tilde{\phi}_l(t)\rangle\}$ . According to Ref. [53], for the nondegenerate eigenvectors  $|\phi_l(t)\rangle$  of a dynamic invariant, the von Neumann equation

$$\frac{d}{dt}\zeta_l(t) = -i[H(t), \zeta_l(t)], \quad (7)$$

with  $\zeta_l(t) = |\phi_l(t)\rangle\langle\phi_l(t)|$  being naturally satisfied. Therefore, for the computational subspace  $S$  spanned by a set of nondegenerate eigenvectors  $\{|\phi_l(t)\rangle\}$  of a dynamic invariant, the satisfaction of the von Neumann equation does not need to be verified again. To realize NHQC, it is only necessary to eliminate the dynamic part of the Lewis-Riesenfeld phase obtained in  $[0, T]$  as

$$\vartheta_l(T) = -\int_0^T \langle \phi_l(t) | H(t) | \phi_l(t) \rangle dt = 0. \quad (8)$$

In this case, the remaining part of Lewis-Riesenfeld phase,

$$\Theta_l(T) = \int_0^T \langle \phi_l(t) | i\frac{\partial}{\partial t} | \phi_l(t) \rangle dt, \quad (9)$$

is purely geometric.

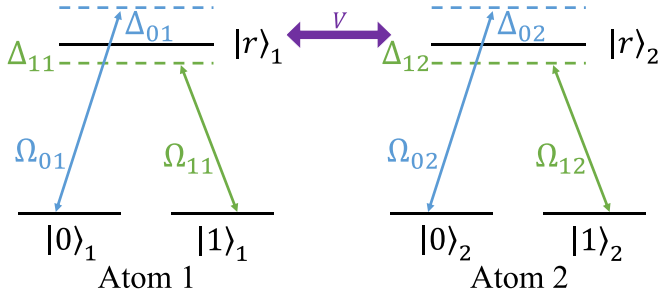


FIG. 1. Level configuration of the computational atom  $k$  ( $k = 1, 2$ ).

### III. SWAP GATE BASED ON NHQC

#### A. Physical model and Hamiltonian

In this section, we introduce a physical model for implementing the SWAP gate with Rydberg atoms. As shown in Fig. 1, the neutral  $^{87}\text{Rb}$  atom  $k$  ( $k = 1, 2$ ) has two ground states,  $|0\rangle_k$  and  $|1\rangle_k$ , and a Rydberg state,  $|r\rangle_k$ . The transition  $|0\rangle_k \leftrightarrow |r\rangle_k$  ( $|1\rangle_k \leftrightarrow |r\rangle_k$ ) is driven by a classical field with Rabi frequency  $\Omega_{0k}$  ( $\Omega_{1k}$ ) and blue (red) detuning  $\Delta_{0k}$  ( $\Delta_{1k}$ ). In addition, the RRI strength is  $V$ . Under the rotating-wave approximation, the Hamiltonian  $H(t)$  of the system takes the following form:

$$H(t) = \sum_{k=1}^2 [\Omega_{0k}(t)e^{-i\Delta_{0k}t}|r\rangle_k\langle 0| + \Omega_{1k}(t)e^{i\Delta_{1k}t}|r\rangle_k\langle 1| + \text{H.c.}] + V|rr\rangle\langle rr|. \quad (10)$$

We consider  $\Delta_{01} = \Delta_{12} + V$  and  $\Delta_{02} = \Delta_{11} + V$  and move into a rotating frame via the unitary operator  $R = \exp(iVt|rr\rangle\langle rr|)$ , giving rise to

$$\begin{aligned} H'(t) &= RH(t)R^\dagger + iR^\dagger \dot{R} \\ &= \Omega_{01}(t)e^{-i(\Delta_{12}+V)t}(|r0\rangle\langle 00| + |r1\rangle\langle 01|) \\ &\quad + \Omega_{02}(t)e^{-i(\Delta_{11}+V)t}(|0r\rangle\langle 00| + |1r\rangle\langle 10|) \\ &\quad + \Omega_{01}(t)e^{-i\Delta_{12}t}|rr\rangle\langle 0r| + \Omega_{11}(t)e^{i(\Delta_{11}+V)t}|rr\rangle\langle 1r| \\ &\quad + \Omega_{02}(t)e^{-i\Delta_{11}t}|rr\rangle\langle r0| + \Omega_{12}(t)e^{i(\Delta_{12}+V)t}|rr\rangle\langle r1| \\ &\quad + \Omega_{11}(t)e^{i\Delta_{11}t}(|r0\rangle\langle 10| + |r1\rangle\langle 11|) \\ &\quad + \Omega_{12}(t)e^{i\Delta_{12}t}(|0r\rangle\langle 01| + |1r\rangle\langle 11|) + \text{H.c.} \end{aligned} \quad (11)$$

Under the conditions  $|\Delta_{11} + V|, |\Delta_{12} + V|, |\Delta_{11}|, |\Delta_{12}| \gg |\Omega_{01}(t)|, |\Omega_{02}(t)|$ , by using the second-order perturbation theory [74], the effective Hamiltonian can be calculated as

$$H_{\text{eff}}(t) = \Omega_1(t)|01\rangle\langle rr| + \Omega_2(t)|10\rangle\langle rr| + \text{H.c.}, \quad (12)$$

with

$$\begin{aligned} \Omega_1(t) &= -\Omega_{12}^*(t)\Omega_{01}^*(t)\left(\frac{1}{\Delta_{12}} - \frac{1}{\Delta_{12} + V}\right), \\ \Omega_2(t) &= -\Omega_{11}^*(t)\Omega_{02}^*(t)\left(\frac{1}{\Delta_{11}} - \frac{1}{\Delta_{11} + V}\right). \end{aligned} \quad (13)$$

Here, the Stark shift terms are omitted because they can be eliminated by using auxiliary pulses or levels [23, 75, 76].

In order to implement the holonomic SWAP gate with the Rydberg atoms, we assume  $\Omega_1(t) = \Omega_0(t)\cos\theta$ ,  $\Omega_2(t) =$

$\Omega_0(t)e^{i\varphi}\sin\theta$ , and  $\Omega_0(t) = \tilde{\Omega}_0(t)e^{i\mu(t)}$ . In addition, a set of orthogonal basis vectors is defined as  $\{|+\rangle = \cos\theta|01\rangle + e^{i\varphi}\sin\theta|10\rangle; |-\rangle = \sin\theta|01\rangle - e^{i\varphi}\cos\theta|10\rangle\}$ . In this case, the effective Hamiltonian in Eq. (12) can be rewritten as

$$\begin{aligned} H_g(t) &= \Omega_0(t)|+\rangle\langle rr| + \text{H.c.} \\ &= \Omega_x(t)\sigma_x + \Omega_y(t)\sigma_y + 0 \times \sigma_z, \end{aligned} \quad (14)$$

with  $\Omega_x(t) = \tilde{\Omega}_0(t)\cos[\mu(t)]$ ,  $\Omega_y(t) = \tilde{\Omega}_0(t)\sin[\mu(t)]$ ,  $\sigma_x = |rr\rangle\langle +| + \text{H.c.}$ ,  $\sigma_y = -i|rr\rangle\langle +| + \text{H.c.}$ , and  $\sigma_z = |rr\rangle\langle rr| - |+\rangle\langle +|$ .

#### B. Robust pulse design via invariant-based reverse engineering and optimal control theory

Let us detail the creation of pulse sequences by combining invariant-based reverse engineering and the systematic-error-sensitivity nullified optimal control method [65]. The effective Hamiltonian in Eq. (14) has an SU(2) symmetry dynamic structure. Therefore, the dynamic invariant can be constructed by the superposition of three generators of the SU(2) algebra with time-dependent parameters  $\lambda_x(t)$ ,  $\lambda_y(t)$ , and  $\lambda_z(t)$  [73] as

$$I_g(t) = \lambda_x(t)\sigma_x + \lambda_y(t)\sigma_y + \lambda_z(t)\sigma_z. \quad (15)$$

By inserting the contents of Eqs. (14) and (15) into Eq. (1), we can obtain

$$\begin{aligned} \dot{\lambda}_x(t) &= 2\Omega_y(t)\lambda_z(t), \quad \dot{\lambda}_y(t) = -2\Omega_x(t)\lambda_z(t), \\ \dot{\lambda}_z(t) &= 2\Omega_x(t)\lambda_y(t) - 2\Omega_y(t)\lambda_x(t). \end{aligned} \quad (16)$$

Based on Eq. (16), a constraint equation can be formulated for the coefficients of the dynamic invariant  $I_g(t)$ , expressed as  $\lambda_x^2(t) + \lambda_y^2(t) + \lambda_z^2(t) = C^2$  with a real constant  $C$ . When  $C$  is set to 1, the parameters  $\lambda_x(t)$ ,  $\lambda_y(t)$ , and  $\lambda_z(t)$  can be accordingly defined as

$$\begin{aligned} \lambda_x(t) &= \sin\beta_1 \sin\beta_2, \quad \lambda_y(t) = \sin\beta_1 \cos\beta_2, \\ \lambda_z(t) &= \cos\beta_1, \end{aligned} \quad (17)$$

with  $\beta_1$  and  $\beta_2$  being the time-dependent parameters. According to Eqs. (16) and (17), the solutions of  $\Omega_x(t)$  and  $\Omega_y(t)$  can be obtained as

$$\begin{aligned} \Omega_x(t) &= (\dot{\beta}_2 \sin\beta_2 \tan\beta_1 - \dot{\beta}_1 \cos\beta_2)/2, \\ \Omega_y(t) &= (\dot{\beta}_2 \cos\beta_2 \tan\beta_1 + \dot{\beta}_1 \sin\beta_2)/2. \end{aligned} \quad (18)$$

In addition, the eigenvectors of the dynamic invariant  $I_g(t)$  can also be obtained as [64–66]

$$\begin{aligned} |\phi_g^+(t)\rangle &= \cos\frac{\beta_1}{2}|rr\rangle + ie^{-i\beta_2}\sin\frac{\beta_1}{2}|+\rangle, \\ |\phi_g^-(t)\rangle &= ie^{i\beta_2}\sin\frac{\beta_1}{2}|rr\rangle + \cos\frac{\beta_1}{2}|+\rangle. \end{aligned} \quad (19)$$

The corresponding eigenvalues are 1 and  $-1$ , respectively. According to the results of Eqs. (8) and (9), we can calculate the time derivatives of the dynamic phases and the geometric phases acquired by  $|\phi_g^\pm(t)\rangle$  as follows:

$$\dot{\phi}_g^\pm(t) = \mp \frac{\dot{\beta}_2 \sin^2\beta_1}{2\cos\beta_1}, \quad \dot{\Theta}_g^\pm(t) = \pm \dot{\beta}_2 \sin^2\frac{\beta_1}{2}. \quad (20)$$

To satisfy the cyclic evolution conditions  $|\phi_g^\pm(0)\rangle = |\phi_g^\pm(T)\rangle$  ( $T$  is the total time of evolution), the boundary

condition  $\beta_1(0) = \beta_1(T) = 0$  is needed. Then, to obtain a pure geometric phase, the parameter can be designed as [77]

$$\begin{aligned}\beta_1(t) &= \pi \sin^2(\pi t/T), \\ \beta_2(t) &= -\Theta_g \varepsilon(t) + \tilde{\beta}_2(t), \\ \varepsilon(t) &= \begin{cases} 0, & t \in [0, T/2], \\ 1, & t \in [T/2, T], \end{cases}\end{aligned}\quad (21)$$

where  $\tilde{\beta}_2(t)$  is an undetermined analytic function. With the above assumptions of  $\beta_1(t)$  and  $\beta_2(t)$ , the dynamic phase  $\vartheta_g^-(t)$  is eliminated in the whole evolution process [ $\vartheta_g^-(T) = 0$ ], and the pure geometric phase is  $\Theta_g^-(T) = \Theta_g$  (see Appendix A for details). Therefore, the evolution operator can be described as

$$U_g(T, 0) = e^{i\Theta_g} |+\rangle\langle +| + |-\rangle\langle -|. \quad (22)$$

Furthermore, returning to the computational basis  $\{|00\rangle, |01\rangle, |10\rangle, |11\rangle\}$ , the evolution operator is represented as

$$U_0(\Theta_g, \varphi, \theta) = \begin{pmatrix} 1 & 0 & 0 & 0 \\ 0 & Q & W & 0 \\ 0 & E & R & 0 \\ 0 & 0 & 0 & 1 \end{pmatrix}, \quad (23)$$

with  $Q = e^{i\Theta_g} \cos^2\theta + \sin^2\theta$ ,  $W = e^{-i\varphi}(e^{i\Theta_g} - 1)\cos\theta\sin\theta$ ,  $E = e^{i\varphi}(e^{i\Theta_g} - 1)\cos\theta\sin\theta$ , and  $R = \cos^2\theta + e^{i\Theta_g}\sin^2\theta$ . If we select  $\Theta_g = \pi$ ,  $\varphi = \pi$ , and  $\theta = \pi/4$ , the SWAP gate can be realized, and the gate operator is

$$U_0(\pi, \pi, \pi/4) = \begin{pmatrix} 1 & 0 & 0 & 0 \\ 0 & 0 & 1 & 0 \\ 0 & 1 & 0 & 0 \\ 0 & 0 & 0 & 1 \end{pmatrix}. \quad (24)$$

The boundary conditions of parameters  $\beta_1(t)$  and  $\beta_2(t)$  have already been determined. The next step is to formulate specific expressions for these parameters that will derive the control fields. To realize quantum gates, it is known that the gate fidelities can suffer from systematic errors introduced by parameter imperfections. To mitigate the effects of systematic errors, we can choose parameters  $\beta_1(t)$  and  $\beta_2(t)$  by using the systematic-error-sensitivity nullified optimal method [65]. In the presence of systematic errors with error coefficients  $\eta_0$  and  $\eta_1$  ( $\eta_0, \eta_1 \sim \eta$ ), the Rabi frequencies of the laser pulses become  $\Omega_{0k}(t) \rightarrow (1 + \eta_0)\Omega_{0k}(t)$  and  $\Omega_{1k}(t) \rightarrow (1 + \eta_1)\Omega_{1k}(t)$ . According to Eq. (13), we have  $\Omega_1(t) \rightarrow (1 + \eta_0)(1 + \eta_1)\Omega_1(t) = (1 + \eta_0 + \eta_1)\Omega_1(t) + O(\eta^2)$  and  $\Omega_2(t) \rightarrow (1 + \eta_0)(1 + \eta_1)\Omega_2(t) = (1 + \eta_0 + \eta_1)\Omega_2(t) + O(\eta^2)$ , where  $O(\eta^2)$  denotes terms of order  $\eta^2$  or beyond. Thus, in the presence of systematic errors in the control field, the effective Hamiltonian in Eq. (14) can be rewritten as follows:

$$H_g^\epsilon(t) = (1 + \epsilon)\Omega_0(t)|+\rangle\langle rr| + \text{H.c.}, \quad (25)$$

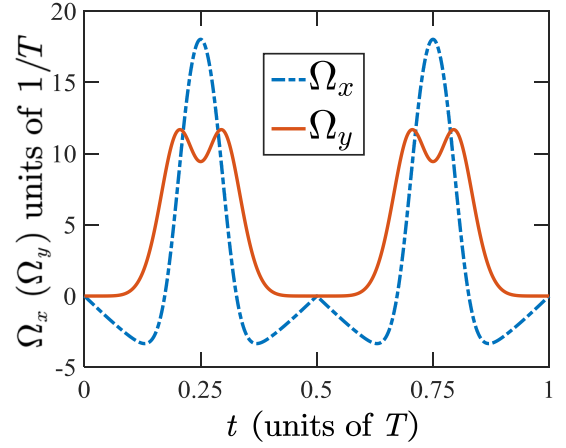


FIG. 2. The control fields  $\Omega_x(t)$  and  $\Omega_y(t)$  versus  $t$ .

where  $\epsilon = \eta_0 + \eta_1$  is the effective error coefficient. By using the time-dependent perturbation theory, we can obtain [65,66]

$$\begin{aligned}|\psi_g^\epsilon(T)\rangle &= |\psi_g(T)\rangle - i\epsilon \\ &\times \int_0^T dt U_g(T, t) H_g(t) |\psi_g(t)\rangle + O(\epsilon^2),\end{aligned}\quad (26)$$

where  $|\psi_g^\epsilon(T)\rangle$  [ $|\psi_g(T)\rangle$ ] denotes the state of the system in the presence (absence) of systematic errors. Since the state  $|-\rangle$  is dynamically decoupled from the Hamiltonian  $H_g(t)$  and the evolution with the initial state  $|+\rangle$  is described by  $|\psi_g(t)\rangle = e^{i\alpha_-(t)}|\phi_g^-(t)\rangle$ , the fidelity of evolution is estimated as

$$F_g = 1 - \epsilon^2 \left| \int_0^T e^{2i\alpha_-(t)} \langle \phi_g^+(t) | H_g(t) | \phi_g^-(t) \rangle dt \right|^2 + O(\epsilon^3), \quad (27)$$

with  $\alpha_+(t) = -\alpha_-(t)$  being considered. Therefore, the systematic error sensitivity  $Q_g$  [65] in this case is calculated as follows:

$$Q_g = -\frac{\partial^2 F_g}{2\partial\epsilon^2} \Big|_{\epsilon=0} = \left| \int_0^T \exp[i\chi(t)] \dot{\beta}_1 \sin^2 \beta_1 dt \right|^2, \quad (28)$$

with  $\chi(t) = \beta_2(t) + 2\alpha_-(t)$ . In order to minimize the influence of system-error sensitivity  $Q_g$ , we select  $\chi(t) = \chi_0\{2\beta_1(t) - 2\sin[2\beta_1(t)]\}$  [65,67] for  $t \in [0, T/2]$ , with  $\chi_0$  being a time-independent parameter. For time node  $t = T/2$ ,  $\chi(t)$  shifts as  $\Delta\chi = \Delta\beta_2 + 2\Delta\Theta_g^- = \Theta_g$ , leading to a modified expression for  $\chi(t)$  as  $\chi(t) = \Theta_g + \chi_0\{2\beta_1(t) - 2\sin[2\beta_1(t)]\}$  for the time range  $[T/2, T]$ . Consequently,  $Q_g$  can be solved as  $Q_g = \sin^2(\chi_0\pi) \sin^2(\Theta_g^2/2)/\chi_0^2$ . If we set  $\chi_0$  as a nonzero integer, the value of  $Q_g$  equals zero, which means that the minimum of the systematic error sensitivity is achieved. Considering that, when we determine the maximum pulse intensity, a larger value of  $\chi_0$  extends the operation time, we select  $\chi_0 = 1$ . Accordingly,  $\beta_2(t)$  is calculated as  $\beta_2(t) = -\Theta_g \varepsilon(t) + 4 \sin^3[\beta_1(t)]/3$  for  $t \in [0, T]$ .

Based on the parameters designed above, we plot the time variations of the control fields  $\Omega_x$  and  $\Omega_y$  in Fig. 2 and obtain the maximum value of the control field  $\Omega_{\max} = \max_{t \in [0, T]} \{|\Omega(t)|\} = 20.35/T$ .

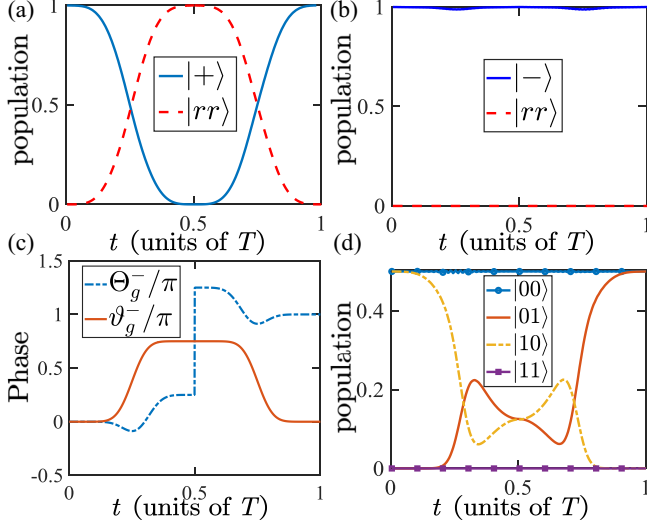


FIG. 3. (a) The time evolution of populations for the states  $|+\rangle$  and  $|rr\rangle$ . (b) The time evolution of populations for the states  $|-\rangle$  and  $|rr\rangle$ . The time evolution of the population is defined as  $P = |\langle \Phi_p | \Phi_0(t) \rangle|^2$ , where  $|\Phi_p\rangle \in \{|+\rangle, |-\rangle, |rr\rangle\}$  is the state corresponding to the evolution of the population and  $\Phi_0(t)$  is the state of the system at time  $t$ . (c) The dynamic phase  $\vartheta_g^-(t)$  and geometric phase  $\Theta_g^-(t)$  in the implementation of the SWAP gate versus  $t$  with the effective Hamiltonian. (d) The time evolution of populations for the computational basis states  $|00\rangle$ ,  $|01\rangle$ ,  $|10\rangle$ , and  $|11\rangle$ . The time evolution of the population is defined as  $P' = |\langle \Phi'_p | \Phi_s(t) \rangle|^2$ , where  $|\Phi'_p\rangle \in \{|00\rangle, |01\rangle, |10\rangle, |11\rangle\}$  is the state corresponding to the evolution of the population and  $\Phi_s(t)$  is the state of system at time  $t$ .

#### IV. NUMERICAL SIMULATIONS AND DISCUSSION

In this section, numerical simulations are used to prove the validity and robustness of the scheme. In order to meet the conditions  $\{|\Delta_{11} + V|, |\Delta_{12} + V|, |\Delta_{11}|, |\Delta_{12}| \gg |\Omega_{01}(t)|, |\Omega_{02}(t)|\}$ , we choose  $V = 5000/T$ ,  $\Delta_{11} = \Delta_{12} = 1700/T$ , and  $\Delta_{01} = \Delta_{02} = 6700/T$ . The solutions of the Rabi frequencies of the classical fields are given in Appendix B. Considering an experimental reported Rydberg interaction strength  $V = 2\pi \times 50$  MHz [63,76,78], where the distance between the centers of Rydberg atoms is about  $d = 3.755$   $\mu\text{m}$  with the van der Waals coefficient  $C_6 = 8.8 \times 10^{11}$   $\mu\text{m}^6/\text{s}$  [79,80], the total time of system evolution is  $T = 15.92$   $\mu\text{s}$ . Under the current parameter conditions, the scheme is numerically simulated and discussed.

##### A. The validity of the scheme

Before the robustness analysis of the scheme, it is necessary to verify the validity of the effective Hamiltonian in Eq. (14). In Figs. 3(a) and 3(b), we plot the time evolution of populations for the states  $|+\rangle$ ,  $|-\rangle$ , and  $|rr\rangle$  using the full Hamiltonian in Eq. (10). In Fig. 3(a), during the evolution period, the states  $|+\rangle$  and  $|rr\rangle$  experience population transfer and finally return to the initial population. In Fig. 3(b), due to the dynamical decoupling of states  $|-\rangle$  and  $|rr\rangle$ , the populations of the two states remain unchanged during the evolution. It can be seen that the results shown in Fig. 3(b) are in good agreement with the expectations. Moreover, the dynamic

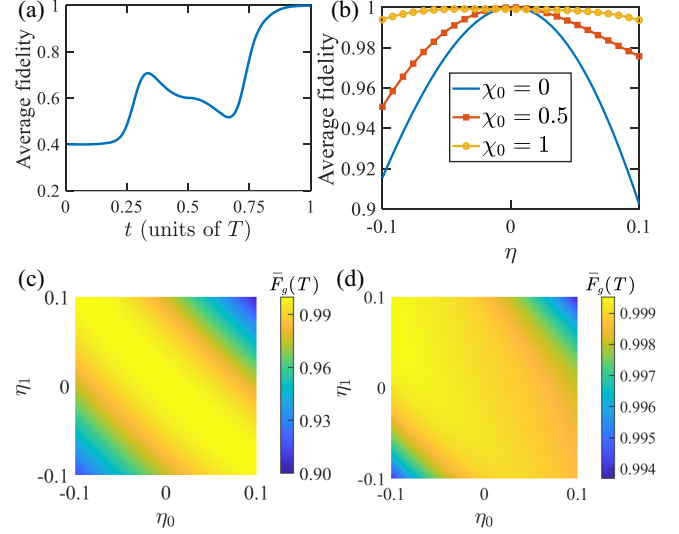


FIG. 4. (a) The average fidelity  $\bar{F}_g^-(t)$  of the holonomic SWAP gate versus  $t$  with the full Hamiltonian. (b) The final average fidelity  $\bar{F}_g^-(T)$  versus the systematic error coefficient for different parameters  $\chi_0$  with  $\eta_0 = \eta_1 = \eta$ . (c) The final average fidelity  $\bar{F}_g^-(T)$  versus  $\eta_0$  and  $\eta_1$  with  $\chi_0 = 0$ . (d) The final average fidelity  $\bar{F}_g^-(T)$  versus  $\eta_0$  and  $\eta_1$  with  $\chi_0 = 1$ .

phase  $\vartheta_g^-(t)$  and geometric phase  $\Theta_g^-(t)$  acquired during the evolution are shown in Fig. 3(c). From Fig. 3(c), it can be observed that the dynamic phase  $\vartheta_g^-(t)$  gradually vanishes as  $t$  approaches  $T$ , whereas the geometric phase  $\Theta_g^-(t)$  obtains a predetermined value of  $\Theta_g^-(T) = \Theta_g = \pi$  at time  $T$ . This indicates that the evolution leads to the acquisition of a purely geometric phase.

Finally, we choose a special initial state  $|\Phi_s(0)\rangle = \frac{1}{\sqrt{2}}(|00\rangle + |10\rangle)$  to verify the validity of the holonomic SWAP gate. Correspondingly, the target state is  $|\Phi_s(T)\rangle = \frac{1}{\sqrt{2}}(|00\rangle + |01\rangle)$ . The populations of the computational basis states  $|00\rangle$ ,  $|01\rangle$ ,  $|10\rangle$ , and  $|11\rangle$  are shown in Fig. 3(d). It can be seen that the populations of states  $|00\rangle$  and  $|11\rangle$  remain unchanged, while states  $|01\rangle$  and  $|10\rangle$  accomplish a population inversion. Therefore, based on the above analysis, we verify the validity of the effective Hamiltonian in Eq. (14), and the holonomic SWAP gate can be successfully realized.

##### B. The robustness of the scheme

To estimate the performance of the holonomic SWAP gate with different initial states, we define the average fidelity for all possible initial states as [81,82]

$$\bar{F}_g^-(t) = \frac{1}{\mathcal{N}(\mathcal{N} + 1)} \{ \text{Tr}[M(t)M^\dagger(t)] + |\text{Tr}[M(t)]|^2 \}, \quad (29)$$

where  $M(t) = P_c U_{\text{SWAP}}^\dagger U(t) P_c$ ,  $U_{\text{SWAP}} = |00\rangle\langle 00| + |10\rangle\langle 01| + |01\rangle\langle 10| + |11\rangle\langle 11|$ ,  $P_c = |00\rangle\langle 00| + |01\rangle\langle 01| + |10\rangle\langle 10| + |11\rangle\langle 11|$  is the projection operator onto the computational subspace, and  $\mathcal{N} = 4$  represents the dimension of the computational subspace. The average fidelity  $\bar{F}_g^-(t)$  versus  $t$  calculated with the full Hamiltonian in Eq. (10) is plotted in Fig. 4(a). According to Fig. 4(a), the average

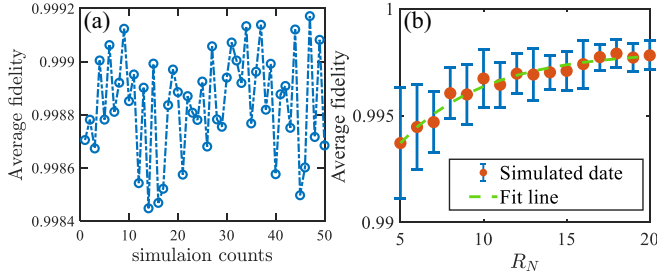


FIG. 5. (a) The final average fidelity  $\bar{F}_g(T)$  versus simulation counts under AWGN with SNR  $R_N = 10$ . (b) The average fidelity versus SNR  $R_N$ . The green dashed line exhibits the fitting results based on  $\ln[1 - \bar{F}_g(T)] \propto -R_N$ .

fidelity of the holonomic SWAP gate is  $\bar{F}_g(T) = 0.9991$  at  $t = T$ , which is in accordance with the expectation.

Taking into account the systematic error of the laser pulse, we plot the final average fidelity  $\bar{F}_g(T)$  of the SWAP gate versus the systematic error coefficient with the parameters  $\chi_0 = 0$ ,  $\chi_0 = 0.5$ , and  $\chi_0 = 1$  in Fig. 4(b). As shown in Fig. 4(b), when the systematic error sensitivity is completely eliminated ( $\chi_0 = 1$ ), the average fidelity of the SWAP gate is  $\bar{F}_g(T) > 0.9937$  when  $\eta \in [-0.1, 0.1]$ , which shows that the scheme is insensitive to systematic error. It can also be observed that the final average fidelity drops to  $\bar{F}_g(T) = 0.9025$  when  $\eta = 0.1$  with  $\chi_0 = 0$ , i.e., without the optimal control [37,83–86]. Next, we show the relationships of the final average fidelity  $\bar{F}_g(T)$  versus  $\eta_0$  and  $\eta_1$  with the parameters  $\chi_0 = 0$  and  $\chi_0 = 1$  in Figs. 4(c) and 4(d), respectively. Figures 4(c) and 4(d) show more clearly that the scheme using the optimal control is more robust to systematic errors. That is, with the help of invariant-based reverse engineering and the systematic-error-sensitivity nullified optimal method, the robustness of the scheme against the systematic errors of laser pulses is greatly enhanced.

In addition to systematic error, random noise is also an inevitable factor in practical experiments. In order to simulate the influence of various random processes, the additive white Gaussian noise (AWGN) [53,87–89] is selected as a typical noise model. Here, we use AWGN to evaluate the performance of the scheme in a noisy environment. The actual Rabi frequency under the influence of AWGN is

$$\begin{aligned}\Omega'_{0k}(t) &= \Omega_{0k}(t) + N_{\text{AWG}}(\Omega_{0k}(t), R_N), \\ \Omega'_{1k}(t) &= \Omega_{1k}(t) + N_{\text{AWG}}(\Omega_{1k}(t), R_N),\end{aligned}\quad (30)$$

where  $N_{\text{AWG}}(\Omega_{0k}(t), R_N)$  [ $N_{\text{AWG}}(\Omega_{1k}(t), R_N)$ ] denotes a function generating AWGN with the signal-to-noise ratio (SNR)  $R_N$  for the control field  $\Omega_{0k}(t)$  [ $\Omega_{1k}(t)$ ]. Because random noise shows different effects in two separate simulations, in order to estimate the impact of AWGN, multiple numerical simulations should be carried out. We performed 50 simulations for the final average fidelity  $\bar{F}_g(T)$  with SNR  $R_N = 10$ , and the results are shown in Fig. 5(a). According to Fig. 5(a), in the presence of AWGN, the final average fidelity fluctuates in a very small range (the fluctuation range does not exceed 0.0008). For 50 simulations, the average fidelity is higher than 0.9984. Meanwhile, in Fig. 5(b), we show the average fidelity of the SNR from 5 to 20. The error bars (standard deviation) in Fig. 5(b) are obtained by repeating the calculation of the

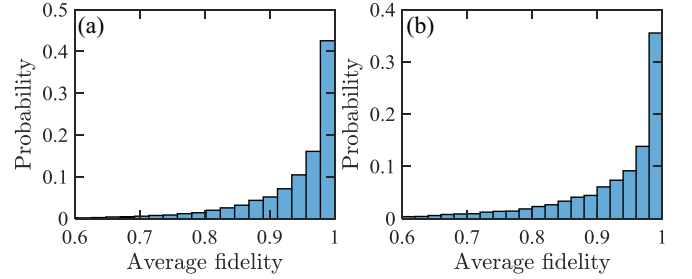


FIG. 6. The distribution of the fidelity  $\bar{F}_g(T)$  when (a) the random initial phase  $\delta_p \in \mathcal{N}(0, \sigma_p^2)$ , with  $\sigma_p = 0.2$ , and (b) the Doppler-shift-inducing detuning  $\delta_D \in \mathcal{N}(0, \sigma_D^2)$ , with  $\sigma_D/(2\pi) = 11.08$  kHz.

average fidelity. The relationship between the average fidelity and SNR  $R_N$  is  $\ln[1 - \bar{F}_g(T)] \propto -R_N$ . The final average fidelity is higher than 0.99 with SNR  $R_N \in [5, 20]$ . Therefore, the results show that the scheme is robust to random noise.

Due to the imperfections of the laser emitter, the laser-induced Rabi oscillations between the ground and excited states of the atom carry a random initial phase. The uncertainty in the initial phase can be modeled by a Gaussian distribution. The random initial phase may occur at each pulse and corresponds to a laser pulse of the form  $\Omega e^{i\delta_p}$ , where  $\delta_p \in \mathcal{N}(0, \sigma_p^2)$  is the Gaussian distribution of the random initial phase and  $\sigma_p^2$  is the variance. We performed 10 000 simulations of the final average fidelity  $\bar{F}_g(T)$  for  $\sigma_p = 0.2$  and plot a histogram of the final average fidelity against its corresponding occurrence probability in Fig. 6(a). According to Fig. 6(a), the results demonstrate that the probability that the final average fidelity is greater than 0.956 is 58.65%, and the average result of 10 000 simulations is 0.9399. On the whole, the scheme still produces acceptable gate fidelity under the influence of random initial phases of pulses.

The Doppler shift caused by fluctuations in the velocity range of atoms due to atomic thermal motion is an important factor that cannot be ignored in experiments. According to concrete reports [90–93], the Doppler shift leads to a random detuning  $\delta_D$  on each atom site, i.e.,  $\delta_D \in \mathcal{N}(0, \sigma_D^2)$ , which is simulated as the error term  $H_D = \delta_D|r\rangle\langle r|$  added to the original Hamiltonian in Eq. (10). The value of  $\delta_D$  is given by  $\sigma_D = k_{\text{eff}} v_{\text{rms}}$ , with  $k_{\text{eff}} = |\mathbf{k}_{|1\rangle \leftrightarrow |e\rangle} + \mathbf{k}_{|e\rangle \leftrightarrow |r\rangle}|$  being the effective wave vector of the two-photon transition  $|1\rangle \leftrightarrow |r\rangle$  and  $v_{\text{rms}} = \sqrt{k_B T/m}$  being the one-dimensional rms velocity spread of atoms. Bringing in the values of the Boltzmann constant  $k_B$ , atomic mass  $m = 87 \times 1.66 \times 10^{-27}$  kg, and atomic temperature  $T = 2 \mu\text{K}$ , we can derive the rms velocity spread  $v_{\text{rms}} = 0.0139$  m/s. Furthermore, we can drive  $|1\rangle \leftrightarrow |e\rangle$  ( $|e\rangle \leftrightarrow |r\rangle$ ) with a 780-nm (480-nm) laser with  $|\mathbf{k}_{|1\rangle \leftrightarrow |e\rangle}| = 2\pi/780 \text{ nm}^{-1}$  ( $|\mathbf{k}_{|e\rangle \leftrightarrow |r\rangle}| = 2\pi/480 \text{ nm}^{-1}$ ). These two lasers can be focused onto the atomic array from opposite directions to minimize the Doppler shift [90], resulting in  $k_{\text{eff}} = 2\pi/480 \text{ nm}^{-1} - 2\pi/780 \text{ nm}^{-1}$  and  $\sigma_D/(2\pi) = 11.08$  kHz. Since the energies of the ground states  $|0\rangle$  and  $|1\rangle$  are close, the Doppler shifts are almost the same for  $|1\rangle \leftrightarrow |r\rangle$  and  $|0\rangle \leftrightarrow |r\rangle$ . Thus, the error term  $H_D = \delta_D|r\rangle\langle r|$  can well describe the Doppler shift effect in the present atomic system. Based on the above descriptions, we performed 10 000

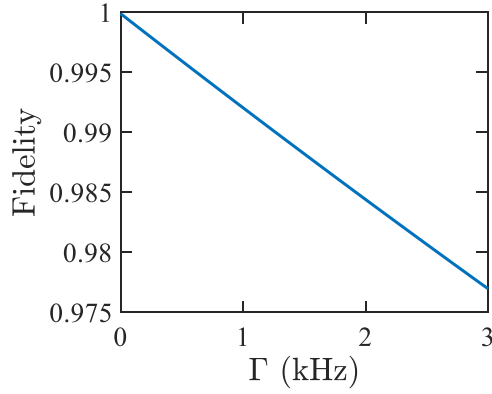


FIG. 7. The final fidelity  $F_g(T)$  of the holonomic SWAP gate versus the atomic decay rate with the initial state  $|\Phi_s(0)\rangle$ .

simulations for the final average fidelity  $\bar{F}_g(T)$  and plot a histogram of the final average fidelity against its corresponding occurrence probability in Fig. 6(b). The average result of 10 000 simulations is 0.9211. Most of the final average fidelity of the simulations lies in the region above 0.9, and the probability that the final average fidelity is greater than 0.96 is even closer to 50%. Therefore, the scheme maintains acceptable gate fidelity even when affected by the Doppler shift.

Decoherence is inevitable for the experimental process. Atomic decay is the main decoherence factor affecting the scheme. Influenced by decoherence, the evolution of the system is governed by a master equation [94] as follows:

$$\begin{aligned} \dot{\rho}(t) = & i[\rho(t), H(t)] \\ & + \sum_{k=1}^2 \sum_{p=0}^1 L_{kp} \rho(t) L_{kp}^\dagger - \frac{1}{2} [L_{kp}^\dagger L_{kp} \rho(t) + \rho(t) L_{kp}^\dagger L_{kp}], \end{aligned} \quad (31)$$

where  $\rho(t)$  is the density operator of the system,  $H(t)$  is the original Hamiltonian,  $k$  is the atomic number, and  $p$  corresponds to the state  $|0\rangle$  or  $|1\rangle$ . In addition, the Lindblad operator  $L_{kp} = \sqrt{\Gamma_{kp}} |p\rangle_k \langle r|$  is the corresponding decay from Rydberg state  $|r\rangle_k$  to the ground state  $|p\rangle_k$ . For simplicity, we assume the atomic decay rate  $\Gamma_{kp} = \Gamma$ .

Similarly, in order to verify the robustness of the holonomic SWAP gate to decoherence, we choose  $|\Phi_s(0)\rangle = \frac{1}{\sqrt{2}}(|00\rangle + |10\rangle)$  as the initial state. We plot the final fidelity  $F_g(T)$  of the holonomic SWAP gate with the initial state  $|\Phi_s(0)\rangle$  versus the atomic decay rate in Fig. 7. The lifetime of the Rydberg state at the principal quantum number of the Rb atom of 70 is around 400  $\mu$ s, which changes to a dissipation coefficient of about 2.5 kHz over here, <3 kHz [95]. For the atomic decay rate from 0 to 3 kHz, the final fidelity  $F_g(T)$  is still very high (above 0.9770). Therefore, the scheme can still work well in the presence of decoherence.

## V. EXTENDING THE SCHEME TO THE NON-CLIFFORD SWAP GATES

According to the evolution operator in Eq. (23), the scheme can be extended to realize the non-Clifford SWAP

gates [96–102]. When  $(\Theta_g, \varphi, \theta) = (\alpha\pi, \pi, \pi/4)$ , we can implement the SWAP $^\alpha$  gate, and the corresponding evolution operator is represented as

$$U_{\text{SWAP}^\alpha} = \begin{pmatrix} 1 & 0 & 0 & 0 \\ 0 & \frac{1}{2}(1 + e^{i\pi\alpha}) & \frac{1}{2}(1 - e^{i\pi\alpha}) & 0 \\ 0 & \frac{1}{2}(1 - e^{i\pi\alpha}) & \frac{1}{2}(1 + e^{i\pi\alpha}) & 0 \\ 0 & 0 & 0 & 1 \end{pmatrix}. \quad (32)$$

When  $\alpha = 1/2$ , the commonly used  $\sqrt{\text{SWAP}}$  gate can be realized. In order to realize the iSWAP gate and the  $\sqrt{\text{iSWAP}}$  gate, a controlled-Z (CZ) gate is required,

$$U_{\text{CZ}}(\Theta_g = \pi, \varphi, \theta = 0) = \begin{pmatrix} 1 & 0 & 0 & 0 \\ 0 & -1 & 0 & 0 \\ 0 & 0 & 1 & 0 \\ 0 & 0 & 0 & 1 \end{pmatrix}, \quad (33)$$

along with the two following steps: (1) performing the CZ gate described above and (2) realizing the iSWAP ( $\sqrt{\text{iSWAP}}$ ) gate by choosing  $(\Theta_g, \varphi, \theta) = (\pi, \pi/2, \pi/4)$  [ $(\Theta_g, \varphi, \theta) = (\pi, \pi/2, \pi/8)$ ]. The evolution operators corresponding to the two gates are as follows:

$$\begin{aligned} U_{\text{iSWAP}} = & U(\pi, \pi/2, \pi/4) U_{\text{CZ}} = \begin{pmatrix} 1 & 0 & 0 & 0 \\ 0 & 0 & i & 0 \\ 0 & i & 0 & 0 \\ 0 & 0 & 0 & 1 \end{pmatrix}, \\ U_{\sqrt{\text{iSWAP}}} = & U(\pi, \pi/2, \pi/8) U_{\text{CZ}} \\ = & \begin{pmatrix} 1 & 0 & 0 & 0 \\ 0 & \frac{1}{\sqrt{2}} & \frac{i}{\sqrt{2}} & 0 \\ 0 & \frac{i}{\sqrt{2}} & \frac{1}{\sqrt{2}} & 0 \\ 0 & 0 & 0 & 1 \end{pmatrix}. \end{aligned} \quad (34)$$

For the implementation of the controlled-SWAP (CSWAP) gate, also known as the Fredkin gate [99,100], we need to add a third atom as the control atom, coupled to the original target atoms 1 and 2, as shown in Fig. 8. The transition  $|0\rangle_3 \leftrightarrow |r\rangle_3$  is driven by a classical field with Rabi frequency  $\Omega_3$  and blue detuning  $\Delta_3$ . The RRI strength between atoms 3 and 1 (3 and 2) is  $V_{13}$  ( $V_{23}$ ). Under the rotating-wave approximation, the Hamiltonian of the system takes the following form:

$$\begin{aligned} H_c(t) = & H(t) \otimes I_3 + I_1 \otimes I_2 \otimes H_3(t) \\ & + V_{13} |r\rangle_1 \langle r| \otimes I_2 \otimes |r\rangle_3 \langle r| + I_1 \otimes V_{23} |rr\rangle_{23} \langle rr|, \end{aligned} \quad (35)$$

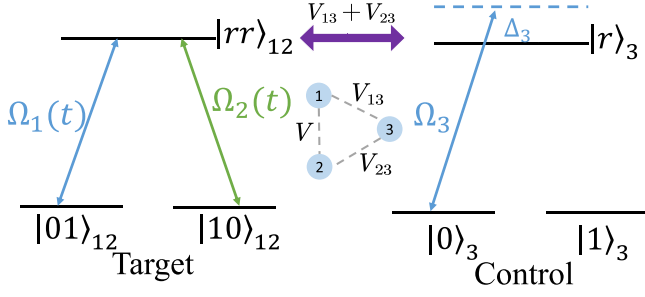


FIG. 8. (a) Schematic for implementing a CSWAP gate. Inset: control atom 3 is coupled to target atoms 1 and 2 described in Fig. 1, with RRI strengths  $V_{13}$  and  $V_{23}$ . The effective  $\Lambda$ -type system of the target atoms is coupled to the control atom with RRI strength  $V_{13} + V_{23}$ .

where  $H(t)$  is given in Eq. (10) and  $H_3(t) = \Omega_3 e^{-i\Delta_3 t} |r\rangle_3 \langle 0| + \text{H.c.}$  Similarly, we consider  $\Delta_{01} = \Delta_{12} + V$ ,  $\Delta_{02} = \Delta_{11} + V$  and move into a rotating frame via the unitary operator  $R_1 = \exp[iVt(|rr0\rangle\langle rr0| + |rr1\rangle\langle rr1|)]$ , giving rise to

$$\begin{aligned} H_{c1}(t) &= R_1 H_c(t) R_1^\dagger + iR_1^\dagger \dot{R}_1 \\ &= H'(t) \otimes I_3 + I_1 \otimes I_2 \otimes H_3(t) + V|rrr\rangle\langle rrr| \\ &\quad + V_{13}(|r0r\rangle\langle r0r| + |r1r\rangle\langle r1r| + |rrr\rangle\langle rrr|) \\ &\quad + V_{23}(|0rr\rangle\langle 0rr| + |1rr\rangle\langle 1rr| + |rrr\rangle\langle rrr|) \\ &\quad + (\Omega_3 e^{-i(\Delta_3+V)t} |rrr\rangle\langle rr0| + \text{H.c.}) \\ &\quad + (-\Omega_3 e^{-i\Delta_3 t} |rrr\rangle\langle rr0| + \text{H.c.}), \end{aligned} \quad (36)$$

where  $H'(t)$  is given in Eq. (11). Like for Eqs. (11) and (12), we can obtain the effective Hamiltonian for the three-atom system from Eq. (36) as

$$\begin{aligned} H_{c2}(t) &= H_{\text{eff}}(t) \otimes I_3 + I_1 \otimes I_2 \otimes H_3(t) + V|rrr\rangle\langle rrr| \\ &\quad + V_{13}(|r0r\rangle\langle r0r| + |r1r\rangle\langle r1r| + |rrr\rangle\langle rrr|) \\ &\quad + V_{23}(|0rr\rangle\langle 0rr| + |1rr\rangle\langle 1rr| + |rrr\rangle\langle rrr|) \\ &\quad + (\Omega_3 e^{-i(\Delta_3+V)t} |rrr\rangle\langle rr0| + \text{H.c.}) \\ &\quad + (-\Omega_3 e^{-i\Delta_3 t} |rrr\rangle\langle rr0| + \text{H.c.}), \end{aligned} \quad (37)$$

where  $H_{\text{eff}}(t)$  is given in Eq. (12). We consider the conditions  $V_{13} = V_{23} = V$ ,  $\Delta_3 = 2V$ , and  $V \gg \Omega_3$ ,  $\Omega_1(t)$ ,  $\Omega_2(t)$  and move into a rotating frame via the unitary operator  $R_2 = \exp(iH_V t)$ , with  $H_V = 3V|rrr\rangle\langle rrr| + V(|r0r\rangle\langle r0r| + |r1r\rangle\langle r1r| + |0rr\rangle\langle 0rr| + |1rr\rangle\langle 1rr|)$ . If we neglect the fast-oscillating terms, the Hamiltonian in Eq. (37) can be simplified as

$$\begin{aligned} H_{c3}(t) &= \Omega_1(t)|010\rangle\langle rr0| + \Omega_2(t)|100\rangle\langle rr0| \\ &\quad + \Omega_1(t)|011\rangle\langle rr1| + \Omega_2(t)|101\rangle\langle rr1| \\ &\quad + \Omega_3|rrr\rangle\langle rr0| + \text{H.c.} \end{aligned} \quad (38)$$

Here, the Stark shift terms are also omitted because they can be eliminated by using auxiliary pulses or levels [23,75,76]. We define  $H_r = \Omega_3|rrr\rangle\langle rr0| + \text{H.c.}$ , whose eigenstates are  $|\tilde{\Phi}_\pm\rangle = (\pm|rr0\rangle + |rrr\rangle)/\sqrt{2}$ , with corresponding eigenvalues of  $\pm\Omega_3$ . Transforming  $H_{c3}(t)$  to the frame defined by

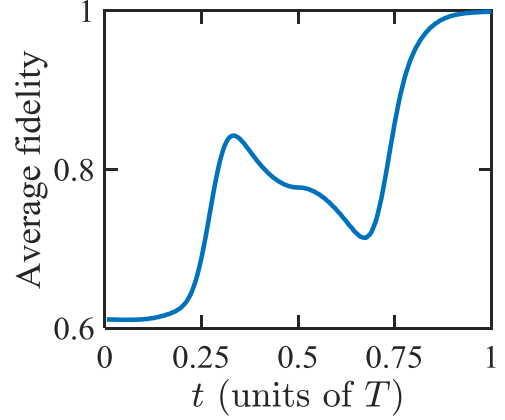


FIG. 9. The average fidelity of the holonomic CSWAP gate versus  $t$  with the full Hamiltonian.

$R' = \exp(iH_r t)$  gives rise to

$$\begin{aligned} H_{c4}(t) &= R' H_{c3}(t) R'^\dagger + iR'^\dagger \dot{R}' \\ &= \frac{1}{\sqrt{2}} [\Omega_1(t)^{-i\Omega_3 t} |010\rangle\langle \tilde{\Phi}_+| - \Omega_1(t)^{i\Omega_3 t} |010\rangle\langle \tilde{\Phi}_-| \\ &\quad + \Omega_2(t)^{-i\Omega_3 t} |100\rangle\langle \tilde{\Phi}_+| - \Omega_2(t)^{i\Omega_3 t} |100\rangle\langle \tilde{\Phi}_-| \\ &\quad + \Omega_1(t)|011\rangle\langle rr1| + \Omega_2(t)|101\rangle\langle rr1| + \text{H.c.}] \end{aligned} \quad (39)$$

Considering the condition  $\Omega_3 \gg \Omega_1(t)$ ,  $\Omega_2(t)$  and, in the case of the large detuning condition, the oscillating terms with frequencies  $\pm\Omega_3$  can be neglected. Therefore, the dynamics of the three atoms can be governed by the effective Hamiltonian

$$H_{CS} = H_{\text{eff}}(t) \otimes |1\rangle_3 \langle 1|. \quad (40)$$

Equation (40) indicates that only when the state of the control atom is  $|1\rangle_3$  does the SWAP gate on atoms 1 and 2 work, which is exactly a CSWAP gate  $U_{\text{CSWAP}} = I_1 \otimes I_2 \otimes |0\rangle_3 \langle 0| + U_0(\pi, \pi, \pi/4) \otimes |1\rangle_3 \langle 1|$ . Finally, we plot the average fidelity of the holonomic CSWAP gate versus  $t$  calculated with the full Hamiltonian in Eq. (35) in Fig. 9. The average fidelity of the CSWAP gate can reach 0.9989 at  $t = T$ , which proves the feasibility of the scheme.

For the  $N$ -atom CSWAP gate, we also perform a brief expansion. The system consists of atoms 1 and 2 as target atoms and atoms  $k'$  ( $k' = 3, 4, \dots, N$ ) as control atoms. The laser drives to the target atoms, and the control atoms are the same as in Fig. 8. However, here, we assume that the individual control atoms simply have Rydberg-Rydberg interactions only with the target atoms and that there are no interactions between the individual control atoms. Under the rotating-wave approximation, the Hamiltonian of the system for  $N$  atoms is as follows:

$$\begin{aligned} H_N(t) &= H(t) \bigotimes_{k'=3}^N I_{k'} + \sum_{k'=3}^N \left[ \bigotimes_{n=1}^{k'-1} I_n \otimes H_{k'}(t) \bigotimes_{n'=k'+1}^N I_{n'} \right] \\ &\quad + \sum_{k'=3}^N \left[ V_{1k'} |r\rangle_1 \langle r| \bigotimes_{n=2}^{k'-1} I_n \otimes |r\rangle_{k'} \langle r| \bigotimes_{l=k'+1}^N I_l \right. \\ &\quad \left. + I_1 \otimes V_{2k'} |r\rangle_2 \langle r| \bigotimes_{n=3}^{k'-1} I_n \otimes |r\rangle_{k'} \langle r| \bigotimes_{l=k'+1}^N I_l \right], \end{aligned} \quad (41)$$



where  $H(t)$  is given in Eq. (10) and  $H_{k'}(t) = \Omega_{k'} e^{-i\Delta_{k'}t} |r\rangle_{k'} \langle 0| + \text{H.c.}$  According to Eqs. (35)–(38), considering the conditions  $V_{1k'} + V_{2k'} = \Delta_{k'}$  and  $V_{1k'}, V_{2k'} \gg \Omega_1(t), \Omega_2(t), \Omega_{k'}$ , we neglect the fast-oscillating terms, and the Hamiltonian in Eq. (41) can be simplified as

$$\begin{aligned} H'_N = & \Omega_1(t) |01\rangle \langle rr| \bigotimes_{k'=3}^N (|1\rangle_{k'} \langle 1| + |0\rangle_{k'} \langle 0|) \\ & + \Omega_2(t) |10\rangle \langle rr| \bigotimes_{k'=3}^N (|1\rangle_{k'} \langle 1| + |0\rangle_{k'} \langle 0|) \\ & + \sum_{k'=3}^N \Omega_{k'} |rr\rangle \langle rr| \bigotimes_{n=3}^{k'-1} I_n \otimes |r\rangle_{k'} \langle 0| \bigotimes_{l=k'+1}^N I_l + \text{H.c.} \end{aligned} \quad (42)$$

According to Eqs. (38)–(40), considering the condition  $\Omega_{k'} \gg \Omega_1(t), \Omega_2(t)$ , we can ignore the high-frequency term from the large detuning condition. Therefore, the dynamics of the  $N$ -atom system is governed by the effective Hamiltonian

$$H_{\text{NCS}} = H_{\text{eff}}(t) \bigotimes_{k'=3}^N |1\rangle_k \langle 1|. \quad (43)$$

Equation (43) indicates that target atoms 1 and 2 execute the SWAP gate only when the states of all control atoms are  $|1\rangle$ .

## VI. CONCLUSION

In conclusion, we proposed a one-step scheme to realize the nonadiabatic holonomic SWAP gate with Rydberg atoms via invariant-based reverse engineering. The physical system contains two Rydberg atoms as the carriers of information. By driving two atoms with large detuned laser pulses, the effective Hamiltonian can be calculated. Subsequently, invariant-based reverse engineering was applied to the effective Hamiltonian with  $\text{SU}(2)$  dynamical structure, and the evolution path of NHQC was constructed. In addition, the systematic-error-sensitivity nullified optimal control method was used in the selection of parameters, which ensured that the scheme is insensitive to the systematic error of pulses. Numerical simulations demonstrated the validity of the scheme and showed that the scheme performs fairly well in the presence of systematic errors, random noise, the random initial phase of the pulses, the Doppler shift, and decoherence. Finally, the scheme was expanded to realize the non-Clifford SWAP gates. Therefore, the scheme may provide some useful perspectives for the realization of SWAP gates and non-Clifford SWAP gates with Rydberg atoms.

## ACKNOWLEDGMENTS

Y.X. was supported by the National Natural Science Foundation of China under Grants No. 11575045 and No. 11874114, the Natural Science Funds for Distinguished Young Scholars of Fujian Province under Grant No. 2020J06011, and a project from Fuzhou University under Grant No. JG2020001-2. Y.-H.C. was supported by the National Natural Science Foundation of China under Grant No. 12304390.

## APPENDIX A: THE DYNAMIC PHASE AND THE GEOMETRIC PHASE OBTAINED FROM THE EVOLUTION PROCESS

Let us describe the calculation of the dynamic phase and geometric phase obtained in the process of evolution. According to Eq. (21),  $\dot{\beta}_2(t)$  can be described by  $\dot{\beta}_2(t) = -\Theta_g \delta(t - T/2) + \tilde{\beta}_2(t)$ , with  $\delta$  being the Dirac delta function. We assume the variation of  $\tilde{\beta}_2(t)$  is symmetrical about  $t = T/2$ , i.e.,  $\tilde{\beta}_2(t) = \tilde{\beta}_2(T - t)$ . Therefore, it can be derived as

$$\dot{\beta}_2(t) = \frac{d\tilde{t}}{dt} \frac{d}{d\tilde{t}} \tilde{\beta}_2(\tilde{t}) = -\dot{\tilde{\beta}}_2(\tilde{t}), \quad (A1)$$

with  $\tilde{t} = T - t$ . For the dynamic phase, we have

$$\begin{aligned} \vartheta_g^-(T) &= - \int_0^T \frac{\dot{\beta}_2(t) \sin^2[\beta_1(t)]}{2 \cos \beta_1(t)} dt \\ &+ \int_0^T \frac{\Theta_g \delta(t - \frac{T}{2}) \sin^2[\beta_1(t)]}{2 \cos \beta_1(t)} dt \\ &= - \int_0^{T/2} \frac{\dot{\beta}_2(t) \sin^2[\beta_1(t)]}{2 \cos \beta_1(t)} dt - \int_{T/2}^T \frac{\dot{\beta}_2(t) \sin^2[\beta_1(t)]}{2 \cos \beta_1(t)} dt \\ &= - \int_0^{T/2} \frac{\dot{\beta}_2(t) \sin^2[\beta_1(t)]}{2 \cos \beta_1(t)} dt - \int_{T/2}^0 \frac{\dot{\beta}_2(\tilde{t}) \sin^2[\beta_1(\tilde{t})]}{2 \cos \beta_1(\tilde{t})} d\tilde{t} \\ &= 0. \end{aligned} \quad (A2)$$

Here, the condition  $\beta_1(T/2) = \pi$  is used. In addition, the geometric phase is

$$\begin{aligned} \Theta_g^-(T) &= - \int_0^T \dot{\beta}_2(t) \sin^2 \frac{\beta_1(t)}{2} dt \\ &+ \int_0^T \Theta_g \delta\left(t - \frac{T}{2}\right) \sin^2 \frac{\beta_1(t)}{2} dt \\ &= \Theta_g - \int_0^{T/2} \dot{\beta}_2(t) \sin^2 \frac{\beta_1(t)}{2} dt \\ &- \int_{T/2}^T \dot{\beta}_2(t) \sin^2 \frac{\beta_1(t)}{2} dt \\ &= \Theta_g - \int_0^{T/2} \dot{\beta}_2(t) \sin^2 \frac{\beta_1(t)}{2} dt \\ &- \int_{T/2}^0 \dot{\beta}_2(\tilde{t}) \sin^2 \frac{\beta_1(\tilde{t})}{2} d\tilde{t} \\ &= \Theta_g. \end{aligned} \quad (A4)$$

## APPENDIX B: SOLUTION OF THE RABI FREQUENCY OF CLASSICAL FIELDS

According to the designed control fields  $\Omega_x(t)$  and  $\Omega_y(t)$ , we can inversely solve the Rabi frequency of the classical field as follows:

$$\Omega_f(t) = - \frac{[\Omega_x(t) + i\Omega_y(t)] \cos\left(\frac{\pi}{4}\right)}{\left(\frac{1}{\Delta_{12}} - \frac{1}{\Delta_{12}+V}\right)},$$

$$\Omega'_f(t) = -\frac{[\Omega_x(t) + i\Omega_y(t)] \sin\left(\frac{\pi}{4}\right) e^{i\pi}}{\left(\frac{1}{\Delta_{11}} - \frac{1}{\Delta_{11+V}}\right)},$$

$$\Omega_{01}(t) = |\Omega_f(t)|^{1/2}, \quad \Omega_{12}(t) = e^{i\nu_1(t)} |\Omega_f(t)|^{1/2},$$

$$\Omega_{02}(t) = |\Omega'_f(t)|^{1/2}, \quad \Omega_{11}(t) = e^{i\nu_2(t)} |\Omega'_f(t)|^{1/2}, \quad (\text{B1})$$

with

$$\nu_1(t) = \arctan \frac{\text{Im}[\Omega_f(t)]}{\text{Re}[\Omega_f(t)]},$$

$$\nu_2(t) = \arctan \frac{\text{Im}[\Omega'_f(t)]}{\text{Re}[\Omega'_f(t)]}. \quad (\text{B2})$$

- 
- [1] G. K. Brennen, C. M. Caves, P. S. Jessen, and I. H. Deutsch, Quantum logic gates in optical lattices, *Phys. Rev. Lett.* **82**, 1060 (1999).
- [2] D. S. Weiss and M. Saffman, Quantum computing with neutral atoms, *Phys. Today* **70**(7), 44 (2017).
- [3] T. F. Gallagher, *Rydberg Atoms* (Cambridge University Press, Cambridge, UK, 1994).
- [4] D. Jaksch, J. I. Cirac, P. Zoller, S. L. Rolston, R. Côté, and M. D. Lukin, Fast quantum gates for neutral atoms, *Phys. Rev. Lett.* **85**, 2208 (2000).
- [5] M. D. Lukin, M. Fleischhauer, R. Cote, L. M. Duan, D. Jaksch, J. I. Cirac, and P. Zoller, Dipole blockade and quantum information processing in mesoscopic atomic ensembles, *Phys. Rev. Lett.* **87**, 037901 (2001).
- [6] E. Urban, T. A. Johnson, T. Henage, L. Isenhower, D. D. Yavuz, T. G. Walker, and M. Saffman, Observation of Rydberg blockade between two atoms, *Nat. Phys.* **5**, 110 (2009).
- [7] A. Gaëtan, Y. Miroshnychenko, T. Wilk, A. Chotia, M. Viteau, D. Comparat, P. Pillet, A. Browaeys, and P. Grangier, Observation of collective excitation of two individual atoms in the Rydberg blockade regime, *Nat. Phys.* **5**, 115 (2009).
- [8] C. Ates, T. Pohl, T. Pattard, and J. M. Rost, Antiblockade in Rydberg excitation of an ultracold lattice gas, *Phys. Rev. Lett.* **98**, 023002 (2007).
- [9] T. Pohl and P. R. Berman, Breaking the dipole blockade: Nearly resonant dipole interactions in few-atom systems, *Phys. Rev. Lett.* **102**, 013004 (2009).
- [10] J. Qian, Y. Qian, M. Ke, X. L. Feng, C. H. Oh, and Y. Z. Wang, Breakdown of the dipole blockade with a zero-area phase-jump pulse, *Phys. Rev. A* **80**, 053413 (2009).
- [11] T. Amthor, C. Giese, C. S. Hofmann, and M. Weidemüller, Evidence of antiblockade in an ultracold Rydberg gas, *Phys. Rev. Lett.* **104**, 013001 (2010).
- [12] W. Li, C. Ates, and I. Lesanovsky, Nonadiabatic motional effects and dissipative blockade for Rydberg atoms excited from optical lattices or microtraps, *Phys. Rev. Lett.* **110**, 213005 (2013).
- [13] S. Basak, Y. Chougale, and R. Nath, Periodically driven array of single Rydberg atoms, *Phys. Rev. Lett.* **120**, 123204 (2018).
- [14] X.-F. Shi, Deutsch, Toffoli, and CNOT gates via Rydberg blockade of neutral atoms, *Phys. Rev. Appl.* **9**, 051001(R) (2018).
- [15] C. P. Shen, J. L. Wu, S. L. Su, and E. J. Liang, Construction of robust Rydberg controlled-phase gates, *Opt. Lett.* **44**, 2036 (2019).
- [16] K. Y. Liao, X. H. Liu, Z. Li, and Y. X. Du, Geometric Rydberg quantum gate with shortcuts to adiabaticity, *Opt. Lett.* **44**, 4801 (2019).
- [17] B. J. Liu, S. L. Su, and M. H. Yung, Nonadiabatic noncyclic geometric quantum computation in Rydberg atoms, *Phys. Rev. Res.* **2**, 043130 (2020).
- [18] S. L. Su, E. J. Liang, S. Zhang, J. J. Wen, L. L. Sun, Z. Jin, and A. D. Zhu, One-step implementation of the Rydberg-Rydberg-interaction gate, *Phys. Rev. A* **93**, 012306 (2016).
- [19] S. L. Su, H. Z. Shen, E. J. Liang, and S. Zhang, One-step construction of the multiple-qubit Rydberg controlled-phase gate, *Phys. Rev. A* **98**, 032306 (2018).
- [20] J. L. Wu, S. L. Su, Y. Wang, J. Song, Y. Xia, and Y. Y. Jiang, Effective Rabi dynamics of Rydberg atoms and robust high-fidelity quantum gates with a resonant amplitude-modulation field, *Opt. Lett.* **45**, 1200 (2020).
- [21] T. H. Xing, X. Wu, and G. F. Xu, Nonadiabatic holonomic three-qubit controlled gates realized by one-shot implementation, *Phys. Rev. A* **101**, 012306 (2020).
- [22] H. D. Yin, X. X. Li, G. C. Wang, and X. Q. Shao, One-step implementation of Toffoli gate for neutral atoms based on unconventional Rydberg pumping, *Opt. Express* **28**, 35576 (2020).
- [23] J. L. Wu, Y. Wang, J. X. Han, Y. K. Feng, S. L. Su, Y. Xia, Y. Y. Jiang, and J. Song, One-step implementation of Rydberg-antiblockade SWAP and controlled-SWAP gates with modified robustness, *Photonics Res.* **9**, 814 (2021).
- [24] C. Dlaska, K. Ender, G. B. Mbeng, A. Kruckenhauser, W. Lechner, and R. van Bijnen, Quantum optimization via four-body Rydberg gates, *Phys. Rev. Lett.* **128**, 120503 (2022).
- [25] M. Gärtner, K. P. Heeg, T. Gasenzer, and J. Evers, Dynamic formation of Rydberg aggregates at off-resonant excitation, *Phys. Rev. A* **88**, 043410 (2013).
- [26] X. F. Shi and Y. Lu, Quantum gates with weak van der Waals interactions of neutral Rydberg atoms, *Phys. Rev. A* **104**, 012615 (2021).
- [27] X. F. Shi, F. Bariani, and T. A. B. Kennedy, Entanglement of neutral-atom chains by spin-exchange Rydberg interaction, *Phys. Rev. A* **90**, 062327 (2014).
- [28] E. Fredkin and T. Toffoli, Conservative logic, *Int. J. Theor. Phys.* **21**, 219 (1982).
- [29] R. Barends *et al.*, Diabatic gates for frequency-tunable superconducting qubits, *Phys. Rev. Lett.* **123**, 210501 (2019).
- [30] W. Ning, X. J. Huang, P. R. Han, H. K. Li, H. Deng, Z. B. Yang, Z. R. Zhong, Y. Xia, K. Xu, D. N. Zheng, and S. B. Zheng, Deterministic entanglement swapping in a superconducting circuit, *Phys. Rev. Lett.* **123**, 060502 (2019).
- [31] N. Sangouard, C. Simon, H. de Riedmatten, and N. Gisin, Quantum repeaters based on atomic ensembles and linear optics, *Rev. Mod. Phys.* **83**, 33 (2011).

- [32] H. Z. Wu, Z. B. Yang, and S. B. Zheng, Quantum state swap for two trapped Rydberg atoms, *Chin. Phys. B* **21**, 040305 (2012).
- [33] A. W. Glaetzle, M. Dalmonte, R. Nath, C. Gross, I. Bloch, and P. Zoller, Designing frustrated quantum magnets with laser-dressed Rydberg atoms, *Phys. Rev. Lett.* **114**, 173002 (2015).
- [34] E. Sjöqvist, D. M. Tong, L. Mauritz Andersson, B. Hessmo, M. Johansson, and K. Singh, Non-adiabatic holonomic quantum computation, *New J. Phys.* **14**, 103035 (2012).
- [35] G. F. Xu, J. Zhang, D. M. Tong, E. Sjöqvist, and L. C. Kwek, Nonadiabatic holonomic quantum computation in decoherence-free subspaces, *Phys. Rev. Lett.* **109**, 170501 (2012).
- [36] P. Z. Zhao, G. F. Xu, and D. M. Tong, Nonadiabatic geometric quantum computation in decoherence-free subspaces based on unconventional geometric phases, *Phys. Rev. A* **94**, 062327 (2016).
- [37] Z. Y. Xue, J. Zhou, and Z. D. Wang, Universal holonomic quantum gates in decoherence-free subspace on superconducting circuits, *Phys. Rev. A* **92**, 022320 (2015).
- [38] Y. M. Wang, Y. Su, X. Chen, and C. F. Wu, Dephasing-protected scalable holonomic quantum computation on a Rabi lattice, *Phys. Rev. Appl.* **14**, 044043 (2020).
- [39] P. Zanardi and M. Rasetti, Holonomic quantum computation, *Phys. Lett. A* **264**, 94 (1999).
- [40] L. A. Wu, P. Zanardi, and D. A. Lidar, Holonomic quantum computation in decoherence-free subspaces, *Phys. Rev. Lett.* **95**, 130501 (2005).
- [41] L. M. Duan, J. I. Cirac, and P. Zoller, Geometric manipulation of trapped ions for quantum computation, *Science* **292**, 1695 (2001).
- [42] J. Pachos, P. Zanardi, and M. Rasetti, Non-Abelian Berry connections for quantum computation, *Phys. Rev. A* **61**, 010305(R) (1999).
- [43] M. V. Berry, Quantal phase factors accompanying adiabatic changes, *Proc. R. Soc. London, Ser. A* **392**, 45 (1984).
- [44] Y. Aharonov and J. Anandan, Phase change during a cyclic quantum evolution, *Phys. Rev. Lett.* **58**, 1593 (1987).
- [45] E. Sjöqvist, A new phase in quantum computation, *Physics* **1**, 35 (2008).
- [46] Q. X. Lv, Z. T. Liang, H. Z. Liu, J. H. Liang, K. Y. Liao, and Y. X. Du, Noncyclic geometric quantum computation with shortcut to adiabaticity, *Phys. Rev. A* **101**, 022330 (2020).
- [47] J. Zhang, T. H. Kyaw, D. M. Tong, E. Sjöqvist, and L. C. Kwek, Fast non-Abelian geometric gates via transitionless quantum driving, *Sci. Rep.* **5**, 18414 (2015).
- [48] S. L. Zhu and P. Zanardi, Geometric quantum gates that are robust against stochastic control errors, *Phys. Rev. A* **72**, 020301(R) (2005).
- [49] Z. N. Zhu, T. Chen, X. D. Yang, J. Bian, Z. Y. Xue, and X. H. Peng, Single-loop and composite-loop realization of nonadiabatic holonomic quantum gates in a decoherence-free subspace, *Phys. Rev. Appl.* **12**, 024024 (2019).
- [50] P. Z. Zhao, G. F. Xu, Q. M. Ding, E. Sjöqvist, and D. M. Tong, Single-shot realization of nonadiabatic holonomic quantum gates in decoherence-free subspaces, *Phys. Rev. A* **95**, 062310 (2017).
- [51] B. J. Liu, X. K. Song, Z. Y. Xue, X. Wang, and M. H. Yung, Plug-and-play approach to nonadiabatic geometric quantum gates, *Phys. Rev. Lett.* **123**, 100501 (2019).
- [52] S. Li, T. Chen, and Z. Y. Xue, Fast holonomic quantum computation on superconducting circuits with optimal control, *Adv. Quantum Technol.* **3**, 2000001 (2020).
- [53] Y. H. Kang, Z. C. Shi, B. H. Huang, J. Song, and Y. Xia, Flexible scheme for the implementation of nonadiabatic geometric quantum computation, *Phys. Rev. A* **101**, 032322 (2020).
- [54] Y. X. Du, Z. T. Liang, H. Yan, and S. L. Zhu, Geometric quantum computation with shortcuts to adiabaticity, *Adv. Quantum Technol.* **2**, 1900013 (2019).
- [55] D. Guéry-Odelin, A. Ruschhaupt, A. Kiely, E. Torrontegui, S. Martínez-Garaot, and J. G. Muga, Shortcuts to adiabaticity: Concepts, methods, and applications, *Rev. Mod. Phys.* **91**, 045001 (2019).
- [56] S. Martínez-Garaot, E. Torrontegui, X. Chen, and J. G. Muga, Shortcuts to adiabaticity in three-level systems using lie transforms, *Phys. Rev. A* **89**, 053408 (2014).
- [57] Y. C. Li, D. Martínez-Cercós, S. Martínez-Garaot, X. Chen, and J. G. Muga, Hamiltonian design to prepare arbitrary states of four-level systems, *Phys. Rev. A* **97**, 013830 (2018).
- [58] X. Laforgue, X. Chen, and S. Guérin, Robust stimulated Raman exact passage using shaped pulses, *Phys. Rev. A* **100**, 023415 (2019).
- [59] B. Rousseaux, S. Guérin, and N. V. Vitanov, Arbitrary qudit gates by adiabatic passage, *Phys. Rev. A* **87**, 032328 (2013).
- [60] D. Ran, W. J. Shan, Z. C. Shi, Z. B. Yang, J. Song, and Y. Xia, Pulse reverse engineering for controlling two-level quantum systems, *Phys. Rev. A* **101**, 023822 (2020).
- [61] Y. H. Chen, Z. C. Shi, J. Song, Y. Xia, and S. B. Zheng, Optimal shortcut approach based on an easily obtained intermediate Hamiltonian, *Phys. Rev. A* **95**, 062319 (2017).
- [62] B. H. Huang, Y. H. Kang, Y. H. Chen, Q. C. Wu, J. Song, and Y. Xia, Fast quantum state engineering via universal SU(2) transformation, *Phys. Rev. A* **96**, 022314 (2017).
- [63] R. H. Zheng, Y. H. Kang, D. Ran, Z. C. Shi, and Y. Xia, Deterministic interconversions between the Greenberger-Horne-Zeilinger states and the  $W$  states by invariant-based pulse design, *Phys. Rev. A* **101**, 012345 (2020).
- [64] X. Chen, E. Torrontegui, and J. G. Muga, Lewis-Riesenfeld invariants and transitionless quantum driving, *Phys. Rev. A* **83**, 062116 (2011).
- [65] A. Ruschhaupt, X. Chen, D. Alonso, and J. G. Muga, Optimally robust shortcuts to population inversion in two-level quantum systems, *New J. Phys.* **14**, 093040 (2012).
- [66] X. T. Yu, Q. Zhang, Y. Ban, and X. Chen, Fast and robust control of two interacting spins, *Phys. Rev. A* **97**, 062317 (2018).
- [67] D. Daems, A. Ruschhaupt, D. Sugny, and S. Guérin, Robust quantum control by a single-shot shaped pulse, *Phys. Rev. Lett.* **111**, 050404 (2013).
- [68] L. Van-Damme, D. Schraft, G. T. Genov, D. Sugny, T. Halfmann, and S. Guérin, Robust not gate by single-shot-shaped pulses: Demonstration of the efficiency of the pulses in rephasing atomic coherences, *Phys. Rev. A* **96**, 022309 (2017).
- [69] R. H. Zheng, Y. H. Kang, S. L. Su, J. Song, and Y. Xia, Robust and high-fidelity nondestructive Rydberg parity meter, *Phys. Rev. A* **102**, 012609 (2020).
- [70] H. R. Lewis and W. B. Riesenfeld, An exact quantum theory of the time-dependent harmonic oscillator and of a charged particle in a time-dependent electromagnetic field, *J. Math. Phys.* **10**, 1458 (1969).

- [71] X. Chen and J. G. Muga, Engineering of fast population transfer in three-level systems, *Phys. Rev. A* **86**, 033405 (2012).
- [72] U. Güngördü, Y. Wan, M. A. Fasihi, and M. Nakahara, Dynamical invariants for quantum control of four-level systems, *Phys. Rev. A* **86**, 062312 (2012).
- [73] E. Torrontegui, S. Martínez-Garaot, and J. G. Muga, Hamiltonian engineering via invariants and dynamical algebra, *Phys. Rev. A* **89**, 043408 (2014).
- [74] D. F. James and J. Jerke, Effective Hamiltonian theory and its applications in quantum information, *Can. J. Phys.* **85**, 625 (2007).
- [75] S. L. Su, Y. Tian, H. Z. Shen, H. Zang, E. Liang, and S. Zhang, Applications of the modified Rydberg antiblockade regime with simultaneous driving, *Phys. Rev. A* **96**, 042335 (2017).
- [76] D. X. Li and X. Q. Shao, Unconventional Rydberg pumping and applications in quantum information processing, *Phys. Rev. A* **98**, 062338 (2018).
- [77] Y. H. Kang, Y. Xiao, Z. C. Shi, Y. Wang, J. Q. Yang, J. Song, and Y. Xia, Effective implementation of nonadiabatic geometric quantum gates of cat-state qubits using an auxiliary qutrit, *New J. Phys.* **25**, 033029 (2023).
- [78] T. Wilk, A. Gaëtan, C. Evellin, J. Wolters, Y. Miroshnychenko, P. Grangier, and A. Browaeys, Entanglement of two individual neutral atoms using Rydberg blockade, *Phys. Rev. Lett.* **104**, 010502 (2010).
- [79] Y. M. Liu, X. D. Tian, D. Yan, Y. Zhang, C. L. Cui, and J. H. Wu, Nonlinear modifications of photon correlations via controlled single and double Rydberg blockade, *Phys. Rev. A* **91**, 043802 (2015).
- [80] K. Singer, J. Stanojevic, M. Weidemüller, and R. Côté, Long-range interactions between alkali Rydberg atom pairs correlated to the  $ns$ - $ns$ ,  $np$ - $np$  and  $nd$ - $nd$  asymptotes, *J. Phys. B* **38**, S295 (2005).
- [81] P. Zanardi and D. A. Lidar, Purity and state fidelity of quantum channels, *Phys. Rev. A* **70**, 012315 (2004).
- [82] L. H. Pedersen, N. M. Møller, and K. Mølmer, Fidelity of quantum operations, *Phys. Lett. A* **367**, 47 (2007).
- [83] Z. Y. Xue, J. Zhou, Y. M. Chu, and Y. Hu, Nonadiabatic holonomic quantum computation with all-resonant control, *Phys. Rev. A* **94**, 022331 (2016).
- [84] Z. Y. Xue, F. L. Gu, Z. P. Hong, Z. H. Yang, D. W. Zhang, Y. Hu, and J. Q. You, Nonadiabatic holonomic quantum computation with dressed-state qubits, *Phys. Rev. Appl.* **7**, 054022 (2017).
- [85] P. Z. Zhao, X. D. Cui, G. F. Xu, E. Sjöqvist, and D. M. Tong, Rydberg-atom-based scheme of nonadiabatic geometric quantum computation, *Phys. Rev. A* **96**, 052316 (2017).
- [86] Y. Xu, W. Cai, Y. Ma, X. Mu, L. Hu, T. Chen, H. Wang, Y. P. Song, Z. Y. Xue, Z. Q. Yin, and L. Sun, Single-loop realization of arbitrary nonadiabatic holonomic single-qubit quantum gates in a superconducting circuit, *Phys. Rev. Lett.* **121**, 110501 (2018).
- [87] D. Dong, C. Chen, B. Qi, I. R. Petersen, and F. Nori, Robust manipulation of superconducting qubits in the presence of fluctuations, *Sci. Rep.* **5**, 7873 (2015).
- [88] D. Dong, C. Wu, C. Chen, B. Qi, I. R. Petersen, and F. Nori, Learning robust pulses for generating universal quantum gates, *Sci. Rep.* **6**, 36090 (2016).
- [89] J. L. Wu, Y. Wang, J. X. Han, C. Wang, S. L. Su, Y. Xia, Y. Jiang, and J. Song, Two-path interference for enantiomer-selective state transfer of chiral molecules, *Phys. Rev. Appl.* **13**, 044021 (2020).
- [90] H. Levine, A. Keesling, A. Omran, H. Bernien, S. Schwartz, A. S. Zibrov, M. Endres, M. Greiner, V. Vuletić, and M. D. Lukin, High-fidelity control and entanglement of Rydberg-atom qubits, *Phys. Rev. Lett.* **121**, 123603 (2018).
- [91] S. de Léséleuc, D. Barredo, V. Lienhard, A. Browaeys, and T. Lahaye, Analysis of imperfections in the coherent optical excitation of single atoms to Rydberg states, *Phys. Rev. A* **97**, 053803 (2018).
- [92] J. L. Wu, Y. Wang, J. X. Han, S. L. Su, Y. Xia, Y. Jiang, and J. Song, Resilient quantum gates on periodically driven Rydberg atoms, *Phys. Rev. A* **103**, 012601 (2021).
- [93] R. H. Zheng, S. L. Su, J. Song, W. Li, and Y. Xia, Thermal-dephasing-tolerant generation of mesoscopic superposition states with Rydberg dressed blockade, *Phys. Rev. A* **108**, 042405 (2023).
- [94] M. A. Nielsen and I. L. Chuang, *Quantum Computation and Quantum Information* (Cambridge University Press, Cambridge, 2004).
- [95] I. I. Beterov, I. I. Ryabtsev, D. B. Tretyakov, and V. M. Entin, Quasiclassical calculations of blackbody-radiation-induced depopulation rates and effective lifetimes of Rydberg  $nS$ ,  $nP$ , and  $nD$  alkali-metal atoms with  $n \leq 80$ , *Phys. Rev. A* **79**, 052504 (2009).
- [96] Y. Sung, L. Ding, J. Braumüller, A. Vepsäläinen, B. Kannan, M. Kjaergaard, A. Greene, G. O. Samach, C. McNally, D. Kim, A. Melville, B. M. Niedzielski, M. E. Schwartz, J. L. Yoder, T. P. Orlando, S. Gustavsson, and W. D. Oliver, Realization of high-fidelity CZ and ZZ-free  $i$ SWAP gates with a tunable coupler, *Phys. Rev. X* **11**, 021058 (2021).
- [97] C. K. Hu, J. Yuan, B. A. Veloso, J. Qiu, Y. Zhou, L. Zhang, J. Chu, O. Nurbolat, L. Hu, J. Li, Y. Xu, Y. Zhong, S. Liu, F. Yan, D. Tan, R. Bachelard, A. C. Santos, C. J. Villas-Boas, and D. Yu, Native conditional  $i$ swap operation with superconducting artificial atoms, *Phys. Rev. Appl.* **20**, 034072 (2023).
- [98] M. J. Saarijärvi and E. Sjöqvist,  $i$ SWAP-type geometric gates induced by paths on the Schmidt sphere, *Phys. Rev. A* **109**, 042610 (2024).
- [99] G. J. Milburn, Quantum optical Fredkin gate, *Phys. Rev. Lett.* **62**, 2124 (1989).
- [100] G. L. Jiang, J. B. Yuan, W. Q. Liu, and H. R. Wei, Efficient and deterministic high-dimensional controlled-SWAP gates on hybrid linear optical systems with high fidelity, *Phys. Rev. Appl.* **21**, 014001 (2024).
- [101] K. Koshino, S. Ishizaka, and Y. Nakamura, Deterministic photon-photon  $\sqrt{\text{SWAP}}$  gate using a  $\Lambda$  system, *Phys. Rev. A* **82**, 010301(R) (2010).
- [102] J. H. M. Jensen, J. J. Sørensen, K. Mølmer, and J. F. Sherson, Time-optimal control of collisional  $\sqrt{\text{SWAP}}$  gates in ultracold atomic systems, *Phys. Rev. A* **100**, 052314 (2019).